THE JOURNAL OF PHYSICAL CHEMISTRY A

Article

pubs.acs.org/JPCA

On the Photodetachment from the Green Fluorescent Protein Chromophore

Ksenia B. Bravaya and Anna I. Krylov*

Department of Chemistry, University of Southern California, Los Angeles, California 90089-0482, United States

Supporting Information

ABSTRACT: Motivated by the discrepancies in recent experimental and theoretical studies of photodetachment from isolated model chromophores of the green fluorescent protein (GFP), this study reports calculations of the electron detachment energies and photoelectron spectra of the phenolate and deprotonated *p*-hydroxybenzylidene-2,3-dimethylimidazolinone (HBDI) anions. The spectra were computed using double-harmonic parallel normal mode approximation. High-level coupled-cluster methods as well as density functional theory were used to compute vertical and adiabatic detachment energies of the phenolate anion serving as a model system representing anionic GFP-like chromophores (HBDI). The benchmark calculations reveal that the basis set has significant effect on the computed detachment energies, whereas the results are less sensitive to the level of electron correlation treatment. At least aug-cc-pVTZ basis set is required. The best ωB97X-D and CCSD(T) estimates of phenolate's adiabatic detachment energy are 2.12 and 2.19 eV; these values are very close to the experimental value, 2.253 eV [Gunion et al. *Int. J. Mass Spectrom. Ion Proc.* **1992**, *117*, 601]. The best estimate of the vertical detachment energy of deprotonated HBDI is 2.76 eV, which supports bound character of the bright excited state in the Franck−Condon region. The most intense transition in the computed photoelectron spectra of both phenolate and deprotonated HBDI is the 0−0 S_0−D_0 transition, which is 0.11 eV below vertical detachment energy. Therefore, the position of the maximum of the photoelectron spectrum does not represent vertical detachment energy, and the direct comparison between theory and experiment must involve spectrum modeling.

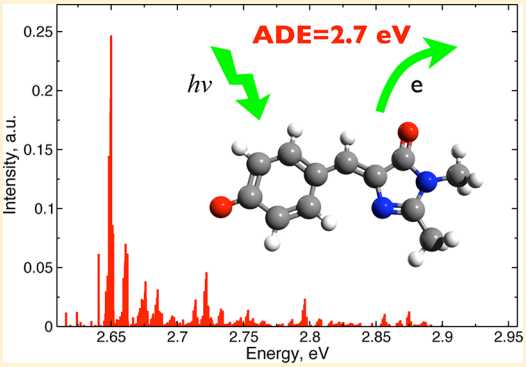

I. INTRODUCTION

Fluorescent proteins (FPs) from the GFP (green FP) family have become indispensable in bioimaging by enabling in vivo studies of subcellular processes. In most applications, FPs are used as genetically encoded inert fluorescent labels. Recently, a new wave of applications has emerged in which FPs are employed as photochemically active players.[1] These novel uses of FPs stem from the two examples of the photochemically active behavior of FPs: the ability of GFP to serve as a photoinduced electron donor[2] and phototoxicity of the KillerRed protein.[3] Understanding the electron-donating ability of the protein-bound GFP chromophore and detailed characterization of the effects of the chromophore−protein interactions can aid the design of FPs with optimized properties for these new applications. The thermodynamics of the electron-donating ability of FPs is characterized by redox potential. Only one theoretical estimate of the standard reduction potentials of an FP is available; for EGFP, the calculations predict E^0 = 0.5 V ($Chro^{\bullet}$ + e → $Chro^{-}$);[4] the experimental value is yet to be determined. However, for model chromophores, the redox potentials have been measured in solutions and compared to calculations.[5,6] Such studies of isolated model chromophores in simple solvents allow one to characterize intrinsic electron-donating ability of the chromophore and to understand how the structure of the chromophore affects its redox potential. Following the reductionist approach, further simplification can be achieved by considering gas-phase model chromophores. Spectroscopic and computational studies of these well-defined simple systems are useful for calibration of theoretical approaches and experimental techniques. Interestingly, the photophysics of the isolated model GFP chromophore is far from being well-understood. The challenge for theory and experiment stems from its anionic nature, which results in closely lying lowest electronically excited state (S_1) and electron-detachment continuum (D_0).[7−14] Consequently, photoexcitation initiates a number of competing deactivation processes: radiationless relaxation (to S_0), photofragmentation, electron emission by direct detachment, resonance autodetachment via S_1, and thermionic emission.[9−13] The relative position of the S_1 and D_0 states also has important implications for electronic structure calculations of the GFP chromophore. The excited states that are metastable with respect to electron detachment (resonances) require special treatment; special techniques developed for the description of excited states lying above photodetachment continuum should be used (see, for

Special Issue: Curt Wittig Festschrift

Received: March 24, 2013
Revised: May 9, 2013
Published: May 10, 2013

example, ref 15 and references therein). Finally, an unambiguous comparison of the experimental measurements and electronic structure calculations must involve spectra modeling. This step is often neglected, leading to misinterpretation of the experimental results.

As illustrated in Figure 1, which shows potential energy curves and a photoelectron spectrum (PES) of a diatomic

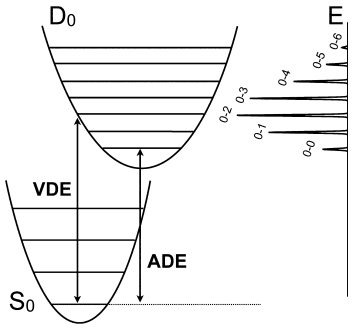

Figure 1. Model ground (S_0) and electron-detached (D_0) states potential energy surfaces (left) and the corresponding photoelectron spectrum (right) for a diatomic molecule (or, more generally, a single Franck–Condon active mode). The most intense vibronic band corresponds to VDE.

molecule, within Franck–Condon (FC) approximation spectral onsets often correspond to the 0–0 transition (adiabatic detachment energy, ADE), and the maxima to the vertical detachment energy (VDE, defined as the difference between electronic energies at the ground-state equilibrium geometry). However, even in diatomic molecules, this picture is not always correct. For example, the FC factor corresponding to the 0–0 transition may become small if photodetachment induces large geometric distortion. Moreover, vibronic interactions between closely lying electronic states may distort the shape of the FC envelope (see, for example, ref 16). In polyatomic molecules, the interpretation of the experimental spectra becomes even more complicated. As our results indicate, in order to extract from the experimental band ADEs and VDEs, one has to model the spectrum. In the discussion below, ADE refers to either computed or experimental adiabatic detachment energy, whereas VDE and λ^d_{max} denote the computed vertical detachment energy and the position of the experimental maximum of the PES, respectively.

The most common model system of the GFP chromophore is *p*-hydroxybenzylidene-2,3-dimethylimidazolinone (HBDI); its deprotonated (anionic) form is shown in Figure 2. Electronic spectra of gas-phase HBDI was first studied by Nielsen et al.[17] by action spectroscopy. By measuring the wavelength dependence of the yield of the photofragmentation products (neutral fragments), the authors reconstructed the photoabsorption spectrum. The reported absorption maximum (λ^a_{max}) was 479 nm (2.59 eV).[7] Electronic structure calculations

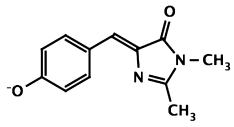

Figure 2. Model GFP chromophore: *p*-hydroxybenzylidene-2,3-dimethylimidazolinone (HBDI). The deprotonated (anionic) form is shown.

of excitation and electron detachment energies by Epifanovsky et al.[7] suggested that the bright excited state of HBDI is a resonance. They reported vertical excitation energy and VDE to be 2.6 and 2.4–2.5 eV, respectively, which rendered the S_1 state as metastable with respect to electron detachment.[7] Forbes and Jockusch were first to report photodetachment from the gas phase HBDI anion and to differentiate photofragmentation and photodetachment channels.[9] The resulting fragment ion action spectrum exhibits a single band with the λ^a_{max} of 482.5 nm (2.57 eV), similar to the spectrum reported by Nielsen et al.[17] The electron detachment signal has two well-defined peaks at 410 (3.02 eV) and 482 nm (2.57 eV), where the first band is due to one-photon absorption and the second involves multiple-photon processes.[9,18]

During the last year, three independent PES studies of the HBDI anion have been published.[10−12] Horke and Verlet[11] reported λ^d_{max} of 2.8 ± 0.1 eV, which makes S_1 bound in the FC region. The PES by Mooney et al.[10] has λ^d_{max} of 2.85 ± 0.1 eV. Slightly red-shifted λ^d_{max} was reported by Toker et al.[12] (2.72 ± 0.1 eV). Interestingly, both band positions and shape of the spectra differ noticeably between the three experiments (see Figure 3). The deviation may be due to slightly different vibrational temperature. In addition, the PES by Mooney et al.[10] shown in Figure 3 was measured at different wavelength (λ = 330 nm) and therefore may reflect additional processes, such as involvement of higher resonance states of the anion. All three groups also reported computed vibrationally resolved PES corresponding to the direct electron detachment. Toker et al.[12] modeled the PES exploiting time-dependent formalism. The resulting spectrum agrees well with the experimental one at λ = 355 nm.[12] The PES by Mooney et al.[10] was simulated using FC factors calculated within double-harmonic parallel normal mode approximation. The spectrum is in a reasonable agreement with the experimental spectrum at λ = 330 nm at the low-energy part of the band, whereas it does not reproduce the higher-energy part of the lowest-energy PES feature. Horke and Verlet[11] reported the PES computed using a similar approach using the Duschinsky rotation scheme. λ^d_{max} of the simulated PES convoluted with Gaussian instrument response function lies between computed ADE and VDE.

This article addresses the following questions: (i) what is the relative position of the S_1 and D_0 states in the FC region; (ii) what is the minimal level of theory required to quantitatively describe energetics of electron detachment in HBDI; and (iii) is it possible to reproduce the shape of the PES of HBDI assuming direct photodetachment and employing double-harmonic parallel normal mode approximation for the FC factors. We use state-of-the-art coupled-cluster methods to characterize photodetachment in the phenolate anion, which can be considered as a model system for HBDI and for which a well-resolved experimental spectrum is available. We benchmark the performance of less computationally expensive DFT and analyze the basis set effects. This validated DFT-based protocol is then applied to study photodetachment in HBDI anion.

The article is organized as follows. We first describe theoretical methods employed (section II). Section III.A summarizes the results of benchmark calculations for the phenolate anion and compares the computed spectrum with the experimental PES. Section III.B presents the energetics of photodetachment in HBDI and the computed PES; it also discusses the comparison to the experiment. Concluding remarks are given in section IV.

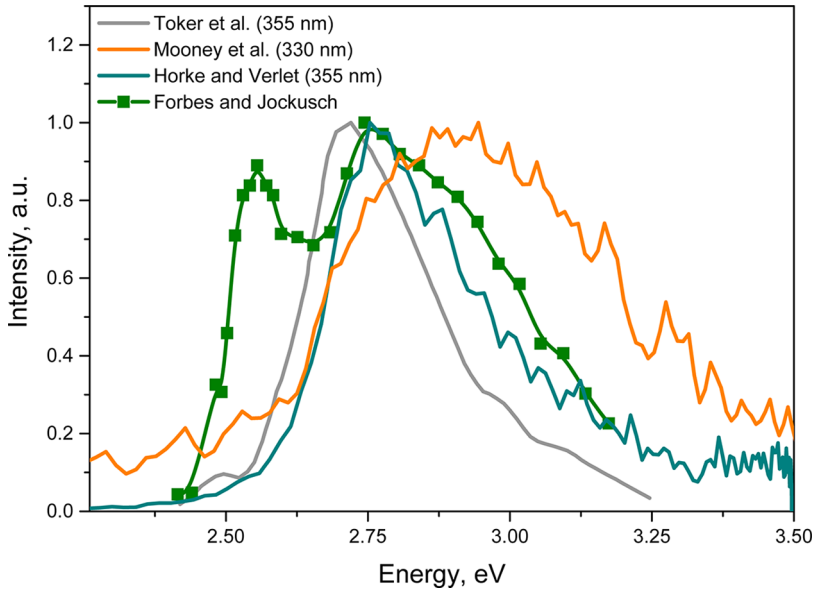

Figure 3. Photoelectron spectra measured at comparable excitation wavelengths as reported by Horke and Verlet,[11] by Mooney et al.,[10] and by Toker et al.[12] The difference in the shape of the PES by Mooney et al.[10] in comparison to the two other PESs can be possibly explained by different excitation wavelength (λ = 330 nm), which may result in population of anion metastable states. Photodetachment signal from the action spectroscopy study by Forbes and Jockusch et al.[9] is also shown. Note that the photodetachment signal from ref 9 cannot be directly compared to PES because photoelectrons with all possible kinetic energies contribute to the former.

II. COMPUTATIONAL DETAILS

Ground-state geometry of the phenolate anion was optimized by RI-MP2 (MP2 with resolution-of-identity[19]) and DFT with the long-range and dispersion-corrected ωB97X-D functional[20] using the cc-pVTZ basis set.[21] The equilibrium geometry of the neutral radical was optimized with ωB97X-D/cc-pVTZ. Single-point energy calculations at the equilibrium geometries of the anion and neutral radical were performed with several coupled-cluster approaches: coupled-cluster with singles and doubles (CCSD), equation-of-motion CCSD for ionization potentials (EOM-IP-CCSD[22−27]), and CCSD with perturbative account of triple substitutions (CCSD(T)[28]). Restricted open-shell Hartree−Fock (ROHF) reference was employed in the CCSD and CCSD(T) energy calculations of the neutral radical. EOM-IP-CCSD does not suffer from spin-contamination as it departs from a well-behaved closed-shell reference for the ground state and describes the target open-shell states by applying 1-hole and 2-hole-1-particle substitution operators to the CCSD reference solution. VDE and ADE for HBDI were computed at the ωB97X-D/cc-pVTZ optimized geometry using ωB97X-D/aug-cc-pVTZ. All electronic structure calculations were performed using the Q-Chem package.[29,30]

The PES of phenolate and HBDI were computed within double harmonic approximation with ωB97X-D/cc-pVTZ harmonic frequencies and normal modes of the anionic and neutral states. Parallel normal mode approximation was employed. The effect of the normal mode mixing on the resulting spectrum was tested by applying the Duschinsky rotation approach.[31−33] Despite strong normal mode mixing manifesting itself in a nondiagonal form of the initial and target states normal modes overlap matrix, there is no notable difference between the spectra computed with parallel normal mode approximation and with Duschinsky rotation. This is because the normal modes that are mixed are not FC-active. Vibrational temperature of the initial state of the anion of 300 K was assumed. The number of maximal vibrational excitation quanta in the initial and target states was limited to 4 and 6, respectively. The vibrational energy of the target state was capped by the 0.3 eV threshold. Thus, transitions with vibrational energy above 0.3 eV in the electron-detached state are not accounted for. The ezSpectrum 3.2 software[34] was used for the PES calculations.

III. RESULTS AND DISCUSSION

A. Photoelectron Spectrum of the Phenolate Anion.

The phenolate anion serves a model system for theoretical studies of the photodetachment from HBDI. Because of its small size and available accurate experimental data, it is possible to quantify the error bars of the electronic structure methods, as well as to test the applicability of approximations used for PES calculations. In addition, there are no low-lying electronically excited states close in energy to the electron detachment threshold (ADE), and therefore, there is no competing autodetachment channel. Hence, only direct detachment contributes to the S_0−D_0 PES.

To determine the level of theory required for accurate prediction of detachment energies, we systematically tested the effects of (i) one-electron basis sets; (ii) treatment of electron correlation; and (iii) equilibrium ground-state geometry. Computed VDEs are summarized in Table 1. To quantify the effects of the basis set, we employed Pople's 6-311(+,+)G(d,p) and Dunning's (aug)-cc-pVNZ up to quadruple-ζ quality bases. As expected, diffuse basis functions are crucial for accurate calculations of electron detachment energies from anions. This can be clearly seen from comparison of EOM-IP-CCSD/cc-pVTZ and EOM-IP-CCSD/aug-cc-pVTZ VDEs: the extension of the basis by adding diffuse functions results in a blue shift of 0.25 eV. The magnitude of the blue shift (~0.2 eV) is almost constant for different methods: DFT with ωB97X-D, EOM-IP-CCSD, CCSD, and CCSD(T). Interestingly, the 6-311(+,+)G(d,p) basis, which is of a triple-ζ quality but has fewer diffuse and polarization functions relative to aug-cc-pVTZ, is

dx.doi.org/10.1021/jp4028904 | J. Phys. Chem. A 2013, 117, 11815−11822

Table 1. S_0-D_0 Vertical Detachment Energies of the Phenolate Anion

method	geometry	VDE (eV)
ωB97X-D/cc-pVTZ	ωB97X-D/cc-pVTZ	2.03
ωB97X-D/aug-cc-pVDZ	ωB97X-D/cc-pVTZ	2.20
ωB97X-D/aug-cc-pVTZ	ωB97X-D/cc-pVTZ	2.20
ωB97X-D/aug-cc-pVQZ	ωB97X-D/cc-pVTZ	2.19
EOM-IP-CCSD/6-311+,+G(d,p)	RIMP2/cc-pVTZ	2.01
EOM-IP-CCSD/cc-pVTZ	RIMP2/cc-pVTZ	2.00
EOM-IP-CCSD/cc-pVTZ	ωB97X-D/cc-pVTZ	1.98
EOM-IP-CCSD/aug-cc-pVDZ	RIMP2/cc-pVTZ	2.08
EOM-IP-CCSD/aug-cc-pVTZ[a]	RIMP2/cc-pVTZ	2.25
CCSD/cc-pVTZ	RIMP2/cc-pVTZ	1.97
CCSD/aug-cc-pVTZ[a]	RIMP2/cc-pVTZ	2.20
CCSD/aug-cc-pVTZ[a]	ωB97X-D/cc-pVTZ	2.18
CCSD(T)/cc-pVTZ	RIMP2/cc-pVTZ	2.01
CCSD(T)/aug-cc-pVTZ[a]	RIMP2/cc-pVTZ	2.27
CCSD(T)/aug-cc-pVTZ[a]	ωB97X-D/cc-pVTZ	2.24

[a]Linear-dependent basis functions were removed. The threshold of 10^{-3} for the eigenvalues of the overlap matrix was used. The resulting number of basis functions is 393.

Table 2. S_0-D_0 Adiabatic Detachment Energies of the Phenolate Anion

method	geometry	ADE (eV)	relaxation energy (eV)
ωB97X-D/cc-pVTZ	ωB97X-D/cc-pVTZ	1.96	0.07
ωB97X-D/aug-cc-pVDZ	ωB97X-D/cc-pVTZ	2.15	0.05
ωB97X-D/aug-cc-pVTZ	ωB97X-D/cc-pVTZ	2.12	0.08
ωB97X-D/aug-cc-pVQZ	ωB97X-D/cc-pVTZ	2.12	0.07
EOM-IP-CCSD/cc-pVTZ	ωB97X-D/cc-pVTZ	1.91	0.07
CCSD/cc-pVTZ	ωB97X-D/cc-pVTZ	1.86	
CCSD/aug-cc-pVTZ[a]	ωB97X-D/cc-pVTZ	2.10	0.08
CCSD(T)/cc-pVTZ	ωB97X-D/cc-pVTZ	1.92	
CCSD(T)/aug-cc-pVTZ[a]	ωB97X-D/cc-pVTZ	2.19	0.05
ΔZPE		+0.01	

[a]Linear-dependent basis functions were removed. The threshold of 10^{-3} for the eigenvalues of the overlap matrix was used. The resulting number of basis functions is 393.

not sufficient: EOM-IP-CCSD/6-311(+,+)G(d,p) VDE of 2.01 eV is blue-shifted by 0.24 eV with respect to the corresponding aug-cc-pVTZ value. This can be explained by the importance of correlation in the ground state wave function of the anion, which is better described using Dunning's correlation-consistent bases. To illustrate the convergence behavior and to test the validity of energy additivity schemes based on the same error due to the basis sets for different methods, we performed calculations in the aug-cc-pVDZ, aug-cc-pVTZ, and aug-cc-pVQZ bases. As one can see, the ωB97X-D results are not sensitive to the basis set extension, whereas EOM-IP-CCSD exhibits notable shift (0.17 eV) in DE upon extension of the basis from aug-cc-pVDZ to aug-cc-pVTZ. The aug-cc-pVDZ basis gives an almost converged VDE value for ωB97X-D, as follows from the comparison between the aug-cc-pVTZ and aug-cc-pVQZ results.

Steep scaling of CCSD and CCSD(T) with the system size (N^6 and N^7, respectively) makes their applications to larger systems (such as HBDI) difficult. Therefore, it is important to quantify the error bars of cheaper approaches, such as DFT. We employ the long-range and dispersion-corrected ωB97X-D functional and use highly accurate CCSD(T) results as a reference to test its performance. As follows from Table 1, ωB97X-D/aug-cc-pVTZ VDE is in excellent agreement with the CCSD(T)/aug-cc-pVTZ value computed at the same ωB97X-D/cc-pVTZ optimized geometry (the deviation of 0.04 eV). Thus, ωB97X-D provides an affordable yet accurate approach that can be used to evaluate VDEs in HBDI and similar chromophores.

The effect of the equilibrium geometry was analyzed by comparing VDEs computed at the ωB97X-D and RI-MP2 optimized geometries (cc-pVTZ basis). The two geometries are very close with the mean absolute deviation in bond lengths of 0.005 Å. Consequently, the effect on computed VDEs is minor: the shift due to the geometry change at the CCSD(T) level is only 0.03 eV.

Thus, ωB97X-D optimized geometries were used to quantify the accuracy of different approaches and basis sets in calculations of ADEs (Table 2) for which the experimental value is available. The basis set effects on computed ADEs are similar to those observed for VDEs: adding the diffuse basis functions to the cc-pVTZ basis results in blue-shift in ADE of 0.16, 0.24, and 0.27 for ωB97X-D, CCSD, and CCSD(T), respectively. Hence, to obtain accurate absolute values of ADEs, one needs to use diffuse basis sets, whereas the relaxation energies (VDE-ADE) are not very sensitive to the diffuseness of the basis. Zero-point vibrational energy correction results in only minor shift in ADE (+0.01 eV). The best estimate of ADE obtained at the CCSD(T)/aug-cc-pVTZ level of theory is 2.19 eV; it is in a very good agreement with the experimental value by Lineberger et al.[35] The ωB97X-D/aug-cc-pVTZ value is red-shifted by 0.13 eV. We expect similar error bars for detachment energies of HBDI.

Phenolate's PES (T = 300 K) computed within double-harmonic parallel normal mode approximation is shown in Figure 4 (top panel). The observed progression corresponds to the ring deformation mode (ν_{11}, Figure 4, top panel). The relaxation from the FC point to the D_0 relaxed geometry results in a large displacement along this normal mode (0.341 Å·amu$^{1/2}$). This can be also clearly seen from the comparison of the equilibrium geometries of the anion and the neutral radical (see Supporting Information, Figure S1). Importantly, the most intense band corresponds to the 0−0 transition, which is red-shifted relative to VDE by 0.05−0.08 eV depending on the level of theory. The computed PES reproduces the shape of the experimental spectrum (Figure 4, bottom panel), including the hot band ($\nu_{11}-0$). Moreover, there is no notable difference in the PES computed within parallel normal mode approximation and Duschinsky rotation scheme (see Supporting Information, Figure S2). In sum, we conclude that ωB97X-D can describe direct detachment energetics and the shape of PES in phenolate and related systems with good accuracy, provided that an appropriate basis set is used.

B. Photoelectron Spectrum of Deprotonated HBDI. Computed VDEs and ADEs as well as the corresponding experimental values are summarized in Table 3. Note that the experimental values are λ^d_{max} of the PES. The estimated experimental ADE reported in ref 11 was derived from linear extrapolation of the low-energy rising edge of the PES band to zero intensity. Therefore, with the current experimental resolution, there is no accurate reference value that can be directly compared to either VDE or ADE. However, both computed quantities are in reasonable agreement with the observed λ^d_{max}. ωB97X-D/aug-cc-pVTZ VDE is 0.26 eV greater

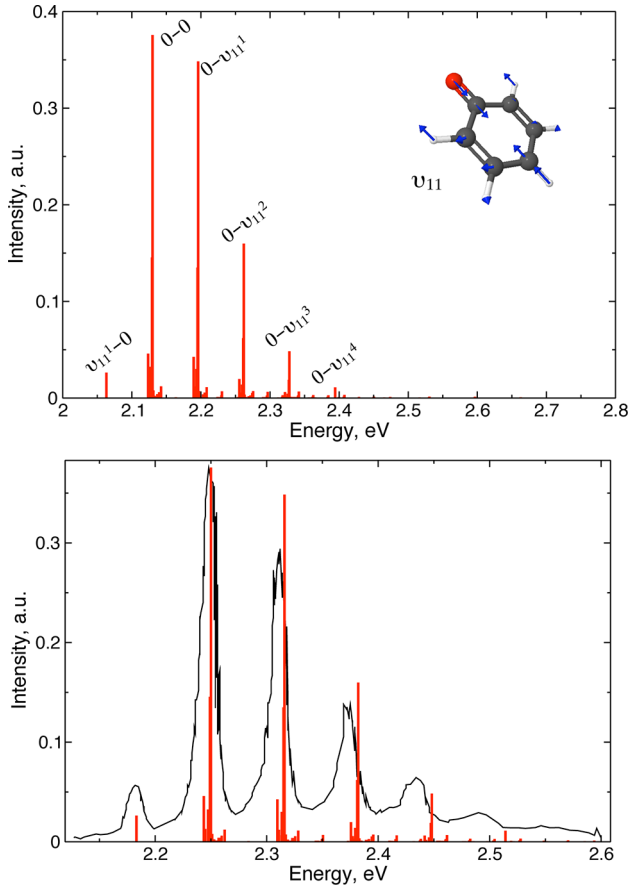

Figure 4. Photoelectron stick spectrum of the phenolate anion computed in double-harmonic parallel normal mode approximation at T = 300K (top panel). Atom displacement vectors corresponding to the active normal mode are also shown. Comparison of the computed and experimental photoelectron spectrum[35] ($T \approx 300$ K) (bottom panel). The computed spectrum is shifted by 0.12 eV so that the maxima of the most intense bands coincide.

than the value reported by Epifanovsky et al.[7] Note that the 2.5 eV value from ref 7 was computed at the CASSCF optimized geometry, which is known to overestimate bond length alternation in conjugated systems.[36] This can lead to notable shifts in computed VDE. However, VDE computed using ωB97X/cc-pVTZ//ωB97X-D/cc-pVTZ coincides with the one reported for the CASSCF structure:[7] ωB97X/cc-pVTZ//CASSCF(14/12)/cc-pVDZ, 2.39 eV. The origin of the discrepancy between the current result (2.76) and the value from ref 7 lies in the choice of the basis set and the extrapolation scheme. The authors assumed identical basis set dependence of VDE computed via Koopmans theorem (KT) and by the correlated EOM-IP-CCSD method. However, KT estimate converges faster with respect to the basis set size than the EOM-IP-CCSD value. For example, KT estimates of the phenolate VDE almost coincide for aug-cc-pVDZ and aug-cc-pVTZ bases: 2.37 and 2.39 eV, respectively (see Supporting Information, Table S1). However, EOM-IP-CCSD values differ significantly: transition from aug-cc-pVDZ to aug-cc-pVTZ increases the VDE from 2.08 to 2.25 eV.

PES computed within double-harmonic parallel normal mode approximation is shown in Figure 5. One can see that the vibrational structure is more complex than in the case of phenolate. However, similarly to the phenolate anion, the most intense band is the 0−0 transition. Therefore, the direct comparison of the λ^d_{max} in the experimental PES and VDE is not justified for this system. However, the two values may numerically coincide due to the line broadening. The most intense transitions in the computed spectrum correspond to the bending vibrations in the HBDI skeleton, in particular, in the imidazolinone and bridge regions that are most strongly affected by the geometry relaxation in the electron-detached state (see Supporting Information, Figure S3). Each line in the stick spectrum has noticeable broadening due to population of the low-frequency modes in the ground electronic state (T = 300 K). As frequencies of these vibrations differ in the S_0 and D_0 states, the transitions conserving the vibrational excitation quanta at these low-frequency modes will be slightly shifted with respect to the parent transition, e.g., 0−0, 0−ν_{50}, etc. As in the phenolate case, using Duschinsky rotation scheme to account for normal mode mixing does not lead to noticeable changes in the spectrum (see Supporting Information, Figure S4).

To compare the computed PES with the experimental one (λ = 355 nm[12]), the stick spectrum was dressed by Gaussians of hwhm (half width at half-maximum) of 0.05 and 0.09 eV

Table 3. Vertical and Adiabatic S_0−D_0 Detachment Energies of the Deprotonated HBDI Anion

method	geometry	VDE (eV)	ADE (eV)	relaxation energy (eV)
ωB97X-D/cc-pVTZ	ωB97X-D/cc-pVTZ	2.65	2.53	0.12
ωB97X-D/aug-cc-pVTZ	ωB97X-D/cc-pVTZ	2.76	2.65	0.11
ΔZPE			2.5×10^{-3}	
B3LYP/6-311(+,+)G(d,p)[9]	B3LYP/6-311(+,+)G(d,p)		2.8	
EPT/aug-cc-pVDZ[10]	TPSSh/6-311(+,+)G(d,p)	2.6		
CAM-B3LYP/aug-cc-pVDZ[11]	CAM-B3LYP/aug-cc-pVDZ	2.79	2.69	0.10
XMCQDPT2/SA(2)-CASSCF(14/14)/[12,37] (p-type d-aug)-cc-pVTZ	PBE0/(aug)-cc-pVDZ	2.62	2.52	0.10
Extrapolated to EOM-IP-CCSD/6-311(2+,+)G(2df,2pd)[7]	CASSCF(14/12)/cc-pVDZ	2.5		
ωB97X/cc-pVDZ	CASSCF(14/12)/cc-pVDZ	2.39		

expt ref	λ^d_{max} (eV)	ADE (eV)
11	2.8	2.6 ± 0.2[a]
10	2.85	
12	2.72	

[a]ADE is determined by a linear extrapolation of the rising edge of the lowest energy PES band.

dx.doi.org/10.1021/jp4028904 | J. Phys. Chem. A 2013, 117, 11815−11822

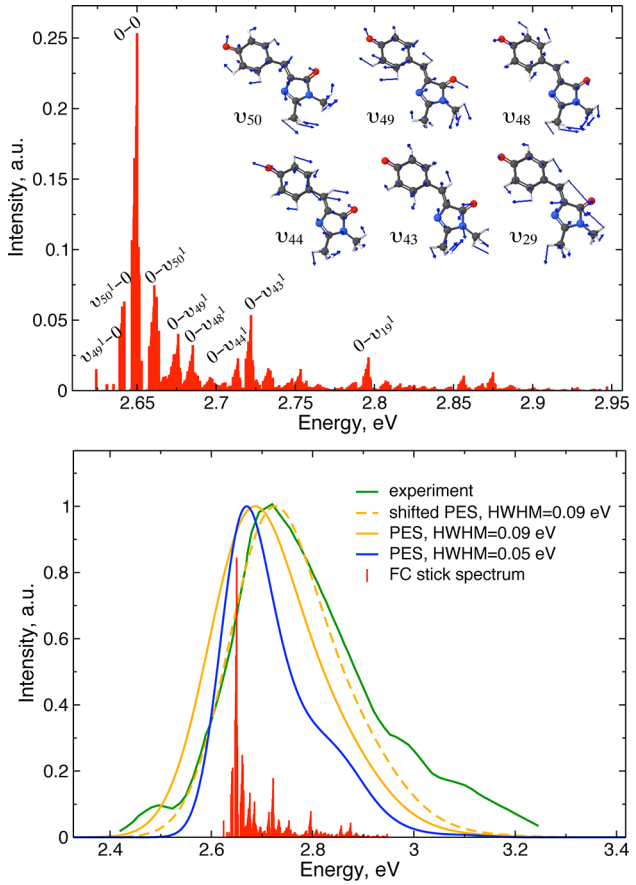

Figure 5. Photoelectron stick spectrum of the HBDI anion computed in double-harmonic parallel normal mode approximation at T = 300 K (top panel). Atoms displacement vectors corresponding to the active normal modes are also shown. Comparison of the computed and experimental photoelectron spectra[12] ($T \approx$ 300 K) (bottom panel).

(Figure 5). One can see that the spectrum corresponding to hwhm of 0.05 nm is significantly more narrow than the experimental one, whereas the one with hwhm = 0.09 eV reproduces the shape of the experimental PES. The latter is clearly seen from the comparison of the computed PES (hwhm = 0.09 eV) shifted by 0.04 eV to the blue so the maximum coincides with the experimental one. Importantly, the maximum is shifted only by 0.04 eV from the ADE, which is less than the VDE−ADE energy difference (0.11 eV). Therefore, the comparison of the computed VDE with the experimental λ^{d}_{max} is misleading in this case. Our spectrum is consistent with the one previously computed as a Fourier transform of Lax's autocorrelation function using PBE0/(aug)-cc-pVDZ optimized geometries and frequencies.[12] It also reproduces the asymmetry of the experimental spectrum: longer and less steep decay toward the higher energies. The difference from the symmetric with respect to the maximum vibronic spectrum reported by Fielding et al.[10] is likely due to the much greater hwhm used for the Gaussians envelope (0.15 eV).

Finally, one may ask a question why in these two systems the most intense transition corresponds to the 0−0 transition, despite significant relaxation in terms of the difference between VDE and ADE. We attribute this to a more delocalized nature of molecular orbitals in polyatomic molecules, which results in smaller geometric distortions along each FC-active mode. Several displacements add up to a substantial energy change; however, the individual displacements are sufficiently small such that the fundamental transition remains the most intense one. This seems to be common in polyatomic molecules, suggesting that the maximum in the absorption/photoelectron spectrum does not necessarily represent vertical excitation/ionization energy and is defined by such factors as density of states, temperature, and line broadening.

IV. CONCLUSIONS

This work presents results of the high-level ab initio benchmark calculations of VDE and ADE of the phenolate anion (serving as a model system representing the HBDI chromophore) and HBDI itself. Analysis of the basis set effects shows that diffuse basis functions are crucial for accurate predictions of detachment energies. In addition, Dunning's aug-cc-pVTZ basis results in better accuracy when used in conjunction with correlated methods, e.g., EOM-IP-CCSD, than Pople's bases of comparable quality (6-311+G(d,p)). We demonstrate that ωB97X-D/aug-cc-pVTZ results in VDE values that are in excellent agreement with CCSD(T)/aug-cc-pVTZ VDE for phenolate: 2.20 and 2.24 eV, respectively. HBDI's VDE and ADE computed with ωB97X-D/aug-cc-pVTZ are 2.76 and 2.65 eV, respectively. Thus, our calculations are in line with the results of several previous experimental and theoretical studies and support bound character of the S_1 state (excitation energy 2.5−2.6 eV[7,9,12,17]) in the FC region. The discrepancy between the current results and previously reported VDE of 2.5 eV[7] is explained.

Phenolate's PES computed within double harmonic parallel normal mode approximation is in excellent agreement with the vibrationally resolved experimental spectrum.[35] The same approach applied to characterize the shape of HBDI PES results in the spectrum consistent with the experimental PES for high photoexcitation energies (λ = 355 nm).

In both systems, the most intense transition corresponds to the 0−0 transition, despite substantial relaxation (in terms of difference between VDE and ADE). Thus, the maximum of the experimental PES does not represent VDE. For phenolate, the computed with CCSD(T) ADE (and, respectively, λ_{max}) is blue-shifted by 0.06 eV relative to the experimental value. In the case of HBDI, the computed values of ADE and VDE are 2.65 and 2.76 eV, respectively. The computed spectrum reproduces the shape of the experimental PES well (λ = 355 nm, ref 12).

■ ASSOCIATED CONTENT

Supporting Information

Equilibrium geometries for the neutral and electron-detached states, harmonic frequencies, comparison of PES computed within parallel normal mode approximation, and Duschinsky rotation for phenolate and HBDI anions. This material is available free of charge via the Internet at http://pubs.acs.org.

■ AUTHOR INFORMATION

Corresponding Author

*(A.I.K.) E-mail: krylov@usc.edu. Phone: (213)740-4929.

Notes

The authors declare no competing financial interest.

■ ACKNOWLEDGMENTS

This work is supported by the Department of Energy through the DE-FG02-05ER15685 grant. A.I.K. also acknowledges

support from the Humboldt Research Foundation (Bessel Award). K.B.B is grateful to Dr. Anastasia Bochenkova for valuable discussions. Authors thank Prof. J. R. R. Verlet and Prof. H. H. Fielding for their feedback on the manuscript.

REFERENCES

(1) Lukyanov, K.; Serebrovskaya, E.; Lukyanov, S.; Chudakov, D. Fluorescent Proteins As Light-Inducible Photochemical Partners. *Photochem. Photobiol. Sci.* **2010**, *9*, 1301−1306.
(2) Bogdanov, A.; Mishin, A.; Yampolsky, I.; Belousov, V.; Chudakov, D.; Subach, F.; Verkhusha, V.; Lukyanov, S.; Lukyanov, K. Green Fluorescent Proteins Are Light-Induced Electron Donors. *Nat. Chem. Biol.* **2009**, *5*, 459−461.
(3) Bulina, M.; Lukyanov, K.; Britanova, O.; Onichtchouk, D.; Lukyanov, S.; Chudakov, D. Chromophore-Assisted Light Inactivation (CALI) Using the Phototoxic Fluorescent Protein KillerRed. *Nat. Protoc.* **2006**, *1*, 947−953.
(4) Bravaya, K.; Khrenova, M.; Grigorenko, B.; Nemukhin, A.; Krylov, A. The Effect of Protein Environment on Electronically Excited and Ionized States of the Green Fluorescent Protein Chromophore. *J. Phys. Chem. B* **2011**, *8*, 8296−8303.
(5) Solntsev, K.; Ghosh, D.; Amador, A.; Josowicz, M.; Krylov, A. What Drives the Redox Properties of Model Green Fluorescence Protein Chromophores? *J. Phys. Chem. Lett.* **2011**, *2*, 2593−2597.
(6) Ghosh, D.; Acharya, A.; Tiwari, S.; Krylov, A. Towards Understanding the Redox Properties of Model Chromophores from the Green Fluorescent Protein Family: An Interplay between Conjugation, Resonance Stabilization, and Solvent Effects. *J. Phys. Chem. B* **2012**, *116*, 12398−12405.
(7) Epifanovsky, E.; Polyakov, I.; Grigorenko, B.; Nemukhin, A.; Krylov, A. Quantum Chemical Benchmark Studies of the Electronic Properties of the Green Fluorescent Protein Chromophore: I. Electronically Excited and Ionized States of the Anionic Chromophore in the Gas Phase. *J. Chem. Theory Comput.* **2009**, *5*, 1895−1906.
(8) Bravaya, K.; Grigorenko, B.; Nemukhin, A.; Krylov, A. Quantum Chemistry Behind Bioimaging: Insights from ab Initio Studies of Fluorescent Proteins and Their Chromophores. *Acc. Chem. Res.* **2012**, *45*, 265−275.
(9) Forbes, M.; Jockusch, R. Deactivation Pathways of an Isolated Green Fluorescent Protein Model Chromophore Studied by Electronic Action Spectroscopy. *J. Am. Chem. Soc.* **2009**, *131*, 17038−17039.
(10) Mooney, C.; Sanz, M.; McKay, A.; Fitzmaurice, R.; Aliev, A.; Caddick, S.; Fielding, H. Photodetachment Spectra of Deprotonated Fluorescent Protein Chromophore Anions. *J. Phys. Chem. A* **2012**, *116*, 7943−7949.
(11) Horke, D. A.; Verlet, J. Photoelectron Spectroscopy of the Model GFP Chromophore Anion. *Phys. Chem. Chem. Phys.* **2012**, *14*, 8511−8515.
(12) Toker, Y.; Rahbek, D.; Klærke, B.; Bochenkova, A.; Andersen, L. Direct and Indirect Electron Emission from the Green Fluorescent Protein Chromophore. *Phys. Rev. Lett.* **2012**, *109*, 128101.
(13) Mooney, C.; Horke, D.; Chatterley, A.; Simperler, A.; Fielding, H.; Verlet, J. Taking the Green Fluorescence out of the Protein: Dynamics of the Isolated GFP Chromophore Anion. *Chem. Sci.* **2013**, *4*, 921−927.
(14) Chingin, K.; Balabin, R.; Frankevich, V.; Barylyuk, K.; Nieckarz, R.; Sagulenko, P.; Zenobi, R. Absorption of the Green Fluorescent Protein Chromophore Anion in the Gas Phase Studied by a Combination of FTICR Mass Spectrometry Withlaser-Induced Photodissociation Spectroscopy. *Int. J. Mass Spectrom.* **2011**, *306*, 241−245.
(15) Bravaya, K.; Zuev, D.; Epifanovsky, E.; Krylov, A. Complex-Scaled Equation-of-Motion Coupled-Cluster Method with Single and Double Substitutions for Autoionizing Excited States: Theory, Implementation, and Examples. *J. Chem. Phys.* **2013**, *138*, 124106.
(16) Stanton, J.; Sattelmeyer, K.; Gauss, J.; Allan, M.; Skalicky, T.; Bally, T. On the Photoelectron Spectrum of *p*-Benzoquinone. *J. Chem. Phys.* **2001**, *115*, 1−4.
(17) Nielsen, S.; Lapierre, A.; Andersen, J.; Pedersen, U.; Tomita, S.; Andersen, L. Absorption Spectrum of the Green Fluorescent Protein Chromophore Anion in vacuo. *Phys. Rev. Lett.* **2001**, *87*, 228102.
(18) Forbes, M.; Nagy, A.; Jocksuch, R. Photofragmentation of and Electron Photodetachment from a GFP Model Chromophore in a Quadrupole Ion Trap. *Int. J. Mass Spectrom.* **20122**, *308*, 155−166.
(19) Weigend, F.; Haser, M. Ri-mp2: First Derivatives and Global Consistency. *Theor. Chim. Acta* **1997**, *208*, 359.
(20) Chai, J.; Head-Gordon, M. Long-Range Corrected Hybrid Density Functionals with Damped Atom−Atom Dispersion Interactions. *Phys. Chem. Chem. Phys.* **2008**, *10*, 6615−6620.
(21) Dunning, T. Gaussian Basis Sets for Use in Correlated Molecular Calculations. I. The Atoms Boron through Neon and Hydrogen. *J. Chem. Phys.* **1989**, *90*, 1007−1023.
(22) Pal, S.; Rittby, M.; Bartlett, R.; Sinha, D.; Mukherjee, D. Multireference Coupled-Cluster Methods Using an Incomplete Model Space: Application to Ionization-Potentials and Excitation-Energies of Formaldehyde. *Chem. Phys. Lett.* **1987**, *137*, 273−278.
(23) Stanton, J.; Gauss, J. Analytic Energy Derivatives for Ionized States Described by the Equation-of-Motion Coupled Cluster Method. *J. Chem. Phys.* **1994**, *101*, 8938−8944.
(24) Kamiya, M.; Hirata, S. Higher-Order Equation-of-Motion Coupled-Cluster Methods for Ionization Processes. *J. Chem. Phys.* **2006**, *125*, 074111−074125.
(25) Pieniazek, P.; Arnstein, S.; Bradforth, S.; Krylov, A.; Sherrill, C. Benchmark Full Configuration Interaction and EOM-IP-CCSD Results for Prototypical Charge Transfer Systems: Noncovalent Ionized Dimers. *J. Chem. Phys.* **2007**, *127*, 164110.
(26) Pieniazek, P.; Bradforth, S.; Krylov, A. Charge Localization and Jahn−Teller Distortions in the Benzene Dimer Cation. *J. Chem. Phys.* **2008**, *129*, 074104.
(27) Krylov, A. Equation-of-Motion Coupled-Cluster Methods for Open-Shell and Electronically Excited Species: The Hitchhiker'S Guide to Fock Space. *Annu. Rev. Phys. Chem.* **2008**, *59*, 433−462.
(28) Raghavachari, K.; Trucks, G.; Pople, J.; Head-Gordon, M. A Fifth-Order Perturbation Comparison of Electron Correlation Theories. *Chem. Phys. Lett.* **1989**, *157*, 479−483.
(29) Shao, Y.; Fusti-Molnar, L.; Jung, Y.; Kussmann, J.; Ochsenfeld, C.; Brown, S.; Gilbert, A.; Slipchenko, L.; Levchenko, S.; O'Neill, D.; DiStasio, R. A., Jr.; Lochan, R. C.; et al. Advances in Methods and Algorithms in a Modern Quantum Chemistry Program Package. *Phys. Chem. Chem. Phys.* **2006**, *8*, 3172−3191.
(30) Krylov, A.; Gill, P. Q-Chem: An Engine for Innovation. *WIREs Comput. Mol. Sci.* **2013**, *3*, 317−326, DOI: 10.1002/wcms.1122.
(31) Kupka, H.; Cribb, P. Multidimensional Franck−Condon Integrals and Duschinsky Mixing Effects. *J. Chem. Phys.* **1986**, *85*, 1303−1315.
(32) Duschinsky, F. On the Interpretation of Electronic Spectra of Polyatomic Molecules. I. Concerning the Franck−Condon Principle. *Acta Physicochim. USSR* **1937**, *7*, 551.
(33) Berger, R.; Fischer, C.; Klessinger, M. Calculation of the Vibronic Fine Structure in Electronic Spectra at Higher Temperatures 1. Benzene and Pyrazine. *J. Phys. Chem. A* **1998**, *102*, 7157−7167.
(34) Mozhayskiy, V.; Krylov, A. ezSpectrum. http://iopenshell.usc.edu/downloads/.
(35) Gunion, R. F.; Gilles, M. K.; Polak, M. L.; Lineberger, W. C. Ultraviolet Photoelectron Spectroscopy of the Phenide, Benzyl and Phenoxide Anions, with ab Initio Calculations. *Int. J. Mass Spectrom. Ion Proc.* **1992**, *117*, 601−620.
(36) Wanko, M.; Hoffmann, M.; Strodel, P.; Koslowski, A.; Thiel, W.; Neese, F.; Frauenheim, T.; Elstner, M. Calculating Absorption Shifts for Retinal Proteins: Computational Challenges. *J. Phys. Chem. B* **2005**, *109*, 3606−3615.
(37) Bochenkova, A.; Andersen, L. Ultrafast Dual Photoresponse of Isolated Biological Chromophores: Link to the Photoinduced Mode-

Specific Non-Adiabatic Dynamics in Proteins. *Faraday Discuss.* **2013**, DOI: 10.1039/C3FD20150C .